Anal. Chem. **1997,** *69,* 2232−2237

Laser-Enhanced Ionization of Mercury Atoms in an Inert Atmosphere with Avalanche Amplification of the Signal

Wendy L. Clevenger, Oleg I. Matveev,† Susana Cabredo,‡ Nicoló Omenetto,§ Benjamin W. Smith, and James D. Winefordner*

Department of Chemistry, University of Florida, Gainesville, Florida 32611-7200

A new method for laser-enhanced ionization detection of mercury atoms in an inert gas atmosphere is described. The method, which is based on the avalanche amplification of the signal resulting from the ionization from a selected Rydberg level reached by a three-step laser excitation of mercury vapor in a simple quartz cell, can be applied to the determination of this element in various matrices by the use of conventional cold atomization techniques. The overall (collisional + photo) ionization efficiency is investigated at different temperatures, and the avalanche amplification effect is reported for Ar and P-10 gases at atmospheric pressure. It is shown that the amplified signal is related to the number of charges produced in the laser-irradiated volume. Under amplifier noise-limited conditions, a detection limit of ∼15 Hg atoms/laser pulse in the interaction region is estimated.

It has been shown[1,2] that, under certain experimental conditions, resonance ionization methods are capable of detecting single atoms in an atmosphere of inert gas or under vacuum. When detecting atoms with ionization techniques in real samples using standard analytical methods for sample atomization (e.g., flames, plasmas, furnaces, or a combination of them), the detection limit depends on the background caused by the number of charged particles in the volume illuminated by laser radiation (the interaction region). For the most part, these particles are created as a result of nonselective laser ionization and thermal ionization of buffer gas or matrix atoms/molecules.[3−6] One way to eliminate the latter factor is to use cold atomization of the sample.

This method is commonly used for the atomization of mercury and is known as cold vapor generation. It involves reducing inorganic Hg in solution to its elemental form and purging the solution with an inert gas. In this way, a stream of inert gas containing the Hg atoms is carried to the detection cell. It was first reported as an atomization source for atomic absorption spectrometry by Hatch and Ott[7] for determination of Hg in water samples. For other elements that are not as volatile at room temperature (including As, Bi, Ge, In, Pb, Sb, Se, Sn, Te, and Tl), the method of hydride generation is widely used to form gaseous analytes.[8]

In addition to cold vapor generation, there are several other methods which involve cold atomization. For example, the sample can be evaporated in a low temperature atomizer or by pulsed or CW laser radiation and the resulting vapor selectively ionized and detected.[9] Using a glow discharge, created by a fast electrical pulse, nonselectively ionized particles can be rapidly removed and the analyte again selectively ionized and detected in a background-free buffer gas.[10]

Compared to other methods, cold atomization can be advantageous in combination with laser ionization spectroscopy techniques as it can lead to a dramatic improvement of the detection limit of the atoms probed by the laser(s) and, consequently, of those present in the original sample. This is due to (1) the elimination of charged background particles due to thermal ionization; (2) the feasibility of an avalanche effect in the buffer gas, which increases the signal by several orders of magnitude;[11] and (3) the fact that because the spectral lines are narrower, less energy is required to saturate transitions at low temperatures. The third advantage is important because low laser irradiance potentially decreases the probability of multiphoton ionization processes in the buffer gas and the resulting high background levels. For these reasons, counting atoms in real samples using cold atomization becomes a real possibility.

The first step in realizing this goal must be the determination of optimal conditions for collisional ionization and photoionization while minimizing the background due to nonselective multiphoton ionization. At the same time, conditions to achieve the optimal avalanche amplification of the signal, while retaining proportionality between the signal and the number of atoms in the interaction region, must be found.

† On leave from the Department of Chemistry, Moscow State University, Moscow, Russia.

‡ On leave from the Department of Chemistry, Universidad de la Rioja, Logroño, Spain.

§ Present address: Environment Institute, Joint Research Centre, Ispra, (Va) Italy.

(1) Hurst, G. S.; Payne, R. B. *Principles and Applications of Resonance Ionization Spectroscopy*; IOP Publishing Ltd.: Bristol, U.K., 1988; pp 50−73.
(2) Letokhov, V. S. *Laser Photoionization Spectroscopy*; Academic Press Inc.: Orlando, FL, 1987; pp 93−116.
(3) Matveev, O. I. *J. Anal. Chem (Russ.)* **1987**, *42*, 1412−8.
(4) Matveev, O. I. *J. Anal. Chem. (Russ.)* **1988**, *43*, 1184−9.
(5) Matveev, O. I.; Omenetto, N. *AIP Conf. Proc.* **1994**, (RIS 94) 515−8.
(6) Turk, G. C. Analytical Performance of Laser-Enhanced Ionization in Flames. In *Laser Enhanced Ionization Spectroscopy*; Travis, J. C., Turk, G. C., Eds.; Wiley Series on Chemical Analysis 136; Winefordner, J. D., Ed.; John Wiley: New York, 1996; pp 161−212.
(7) Hatch, W. R.; Ott, W. L. *Anal. Chem.* **1968**, *40*, 2085−7.
(8) Dědina, J.; Tsalev, D. L. *Hydride Generation Atomic Absorption Spectrometry*; John Wiley: Chichester, U.K., 1995.
(9) Gornushkin, I; Clara, M.; Smith, B. W.; Niessner, R.; Winefordner, J. D., in preparation for publication.
(10) Harrison, W. W.; Hang, W. *Fresenius J. Anal. Chem.* **1996**, *355*, 803−7.
(11) Matveev, O. I.; Smith, B. W.; Omenetto, N.; Winefordner, J. D. *Spectrochim. Acta Part B* **1996**, *51*, 563−7.

S0003-2700(97)00214-X CCC: $14.00

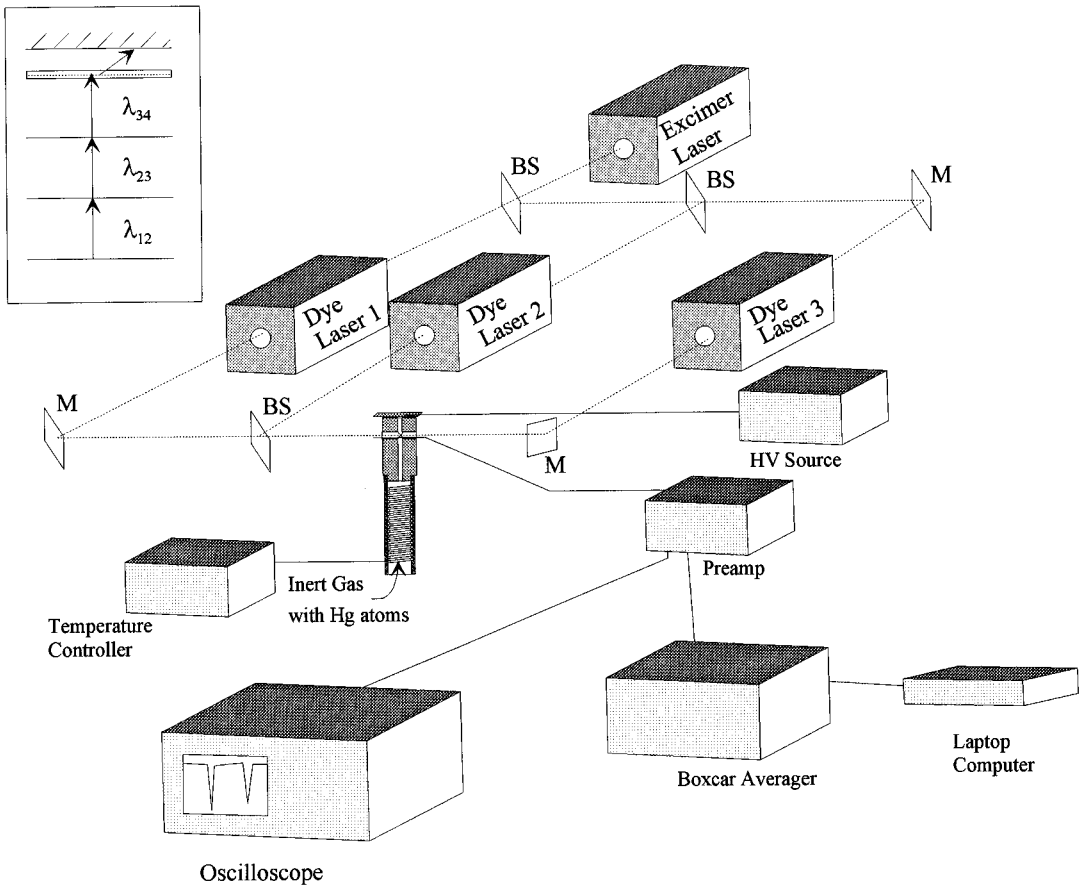

Figure 1. Experimental setup, with the three-step excitation scheme shown in the inset.

The aim of this work is to find these optimal conditions as well as the optimal excitation transitions, laser energy, and electric field that would allow one to reach the ultimate detection limit for mercury atoms in an inert, gaseous environment at ambient temperature.

EXPERIMENTAL SECTION

The experimental setup used in this work, shown in Figure 1 for the sake of clarity, is similar to the one described in our previous paper.[12] The inset gives a schematic representation of the stepwise excitation scheme. Three dye lasers (laser 1, Molectron, Portland, OR; lasers 2 and 3, Model Scanmate 1, Lambda Physik, Acton, MA) were pumped by an excimer laser (Model LPX-240i, Lambda Physik, Acton, MA) operated with XeCl (λ = 308 nm). The transitions to be studied, as tabulated by Moore,[13] are listed in Table 1. The corresponding wavelengths (in air) of the three laser-connected steps were calculated from these transitions. Laser dyes used include Coumarin 500 (Exciton, Dayton, OH), frequency doubled, for λ_{12}; Coumarin 120 (Lambda Physik) for λ_{23}; and Coumarin 153 (Lambda Physik) for the different λ_{34} wavelengths. The frequencies of the first and second lasers remained constant, while the wavelength of the third laser was tuned to levels with different principal quantum numbers. Pulse energies were typically 150 mJ for the excimer, 20 μJ for λ_{12}, 200−300 μJ for λ_{23}, and 0.1−1 mJ for λ_{34}. Laser pulse durations, as reported in our previous work,[12] were ∼34 ns (fwhm).

Table 1. Excitation Transitions for Hg for Laser-Connected Levels 1, 2, 3, and 4 (Rydberg Level)[13]

excitation step	level	energy, cm^{-1}	wavelength, nm
λ_{12}	6p $^3P^0_1$	39 412.3	253.652
λ_{23}	7s $^3S_1$	62 350.5	435.832
λ_{34}	9p $^3P^0_1$	79 412.7	585.925
	9p $^3P^0_1$	79 613.3	579.118
	10p $^3P^0_0$	80 902.27	538.880
	10p $^3P^0_1$	80 916.7	538.463
	10p $^3P^0_2$	81 022.9	535.400
	10p $^1P^0_1$	81 153.6	531.678
	11p $^3P^0_0$	81 800.0	514.012
	11p $^3P^0_1$	81 811.9	513.694
	11p $^3P^0_2$	81 873.8	512.064
	11p $^1P^0_1$	81 942.4	510.270
	12p $^3P^0_1$	82 379.0	499.148
	12p $^3P^0_2$	82 422.6	498.064
	12p $^1P^0_1$	82 464.1	497.037
	13p $^3P^0_1$	82 765.9	489.689
	13p $^3P^0_2$	82 795.0	488.991
	13p $^1P^0_1$	82 823.9	488.300

The beams were directed with mirrors and prisms into the sample cell. This cell is shown in Figure 2 in its two detection configurations. The cell itself was a 15-cm-long, 1-cm-i.d. fused-silica tube plugged at the top with a ceramic stopper, through which a 2-mm hole was bored vertically through the center. The fused-silica tube was connected to an Ar or P-10 gas (90% Ar, 10% CH_4) tank with a small fused-silica reservoir in between. This reservoir contained a small amount of elemental Hg. In this way, inert gas was passed over the liquid Hg at flow rates of 1−100 mL/min, picking up Hg atoms in the vapor phase and carrying

(12) Clevenger, W. L.; Mordoh, L. S.; Matveev, O. I.; Omenetto, N.; Smith B. W.; Winefordner, J. D. *Spectrochim. Acta Part B*, in press.
(13) Moore, C. E. *Atomic Energy Levels*; NSRDS-NBS 35, 1971; Vol. 3, pp 191−5.

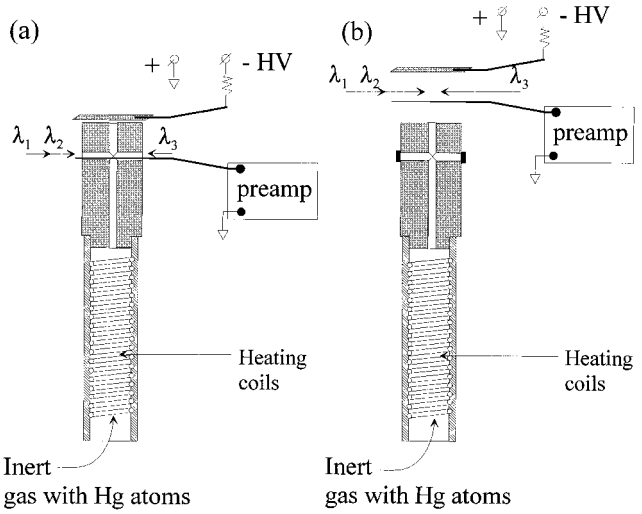

Figure 2. Detection cell. The two electrode configurations used: (a) W collection electrode is contained within the inert gas stream; (b) both electrodes are placed above the cell.

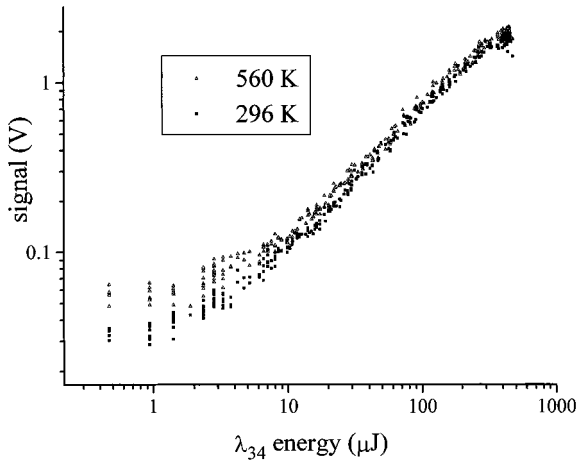

Figure 3. Behavior of the ionization signal vs laser energy for $n = 10$ at room temperature and 550 K.

them through the detection cell. An additional gas line was connected to the output of the Hg reservoir in order to allow dilution of the Hg atoms in the inert gas flow. The laser beams passed through the cell via a 2-mm hole bored horizontally through the ceramic stopper (Figure 2a) or above the stopper, with the horizontal hole covered to prevent loss of analyte (Figure 2b). When the Hg-containing inert gas reached this point, the Hg atoms were selectively ionized and the resulting charges detected by a pair of electrodes.

A planar Ni electrode was connected to a high-voltage source that applied varying potentials (0−3 kV) between the planar electrode and a 0.1-mm-diameter W wire electrode which was connected to a low-noise charge-sensitive preamplifier (Avangard, Inc.). The amplified signal was processed using a boxcar averager (Model SR560, Stanford Research Systems, Sunnyvale CA) and recorded on a lap-top computer. In addition, the amplified ionization wave form was displayed on a fast digitizing oscilloscope (Model 620A, Tektronix, Beaverton, OR).

In order to apply heat to the cell, a heating coil was wrapped around the cell and connected to a variable-voltage transformer. Insulating tape was wrapped around the heating coil. With this system, temperatures up to 550 K could be obtained in the gas volume which was irradiated by the laser. It is important to note that the increase in temperature was not applied to the Hg reservoir since our aim was not that of varying the amount of mercury passing through the cell but rather increasing the number of collisions of the same number of Hg atoms.

In order to attenuate the laser energy of the third laser step, a variable neutral density filter wheel was placed in front of λ_{34}. The wheel was calibrated for λ_{34} before use.

RESULTS AND DISCUSSION

Signal vs Temperature. The ionization signal was first studied as a function of temperature in an attempt to increase the rate of collisional ionization. In the resonance ionization literature,[14] it is well-known that the two factors influencing the rate of collisional ionization are (1) the energy difference between the excited atomic levels of different principal quantum number (from which ionization is occurring) and the ionization continuum and (2) the number of ionizing collisions, which depends on the temperature in and around the interaction region. The former factor was studied in our previous work, in which we observed the behavior of the rate of collisional ionization when different atomic levels, of increasing principal quantum number, were reached by laser excitation.[12]

For the present experiments, the electrode configuration presented in Figure 2b was initially tested. However, a significant loss of signal at higher temperatures was encountered with this setup. These losses were attributed to the quenching of the Hg excited states as a result of the atoms being exposed to air and water vapor molecules. For this reason, the configuration of Figure 2a was used for all subsequent temperature measurements in order to keep the Hg in as inert an atmosphere as possible.

The signal was measured at two temperatures (∼300 and ∼550 K) and for several different final excitation steps (λ_{34}) corresponding to different $7s-np\ ^3P^0_2$ transitions, with n varying from 9 to 13 (see Table 1). In an attempt to differentiate between the mechanisms of photoionization and collisional ionization, the behavior of the signals at these two temperatures as a function of λ_{34} laser energy was investigated by using the variable neutral density filter wheel to attenuate the laser energy. The results for $n = 10$ ($\lambda_{34} = 535.400$) are shown in Figure 3. Clearly, at these temperatures and laser energies, no indication of signal saturation due to the attainment of maximum ionization rates is yet observed. Indeed, even after increasing the energy of the third laser step to values between 0.7 and 0.9 mJ, the data (not reported in Figure 3) did not show a plateau. In addition, at any given value of laser energy, no remarkable difference in the magnitude of the signal, for the two temperatures in the figure, can be seen. Similar behavior was observed for $n = 11$ and $n = 12$.

The dependence of the behavior of the ionization signal on temperature at lower laser irradiances is seen in Figure 4 for $n = 10$, 11, and 12. In this case, a fixed laser energy for λ_{34} of 0.1 mJ was used with a beam that was less tightly focused than for the data shown in Figure 3; therefore, no direct comparison between the two figures should be made. In all the cases shown in Figures 3 and 4, the signals were normalized for thermal expansion. For

(14) Axner, O.; Rubinzstein-Dunlop, H. Fundamental Mechanisms of Laser-Enhanced Ionization: The Production of Atoms. In *Laser Enhanced Ionization Spectroscopy*; Travis, J. C., Turk, G. C., Eds.; Wiley Series on Chemical Analysis 136; Winefordner, J. D., Ed.; John Wiley: New York, 1996; pp 1−98.

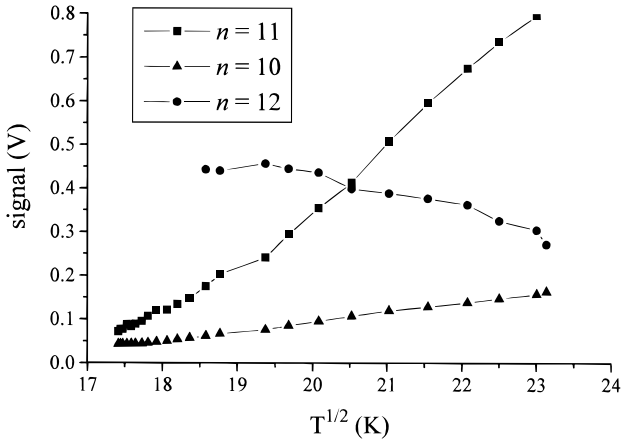

Figure 4. Behavior of the ionization signal vs temperature for n = 10, 11, and 12.

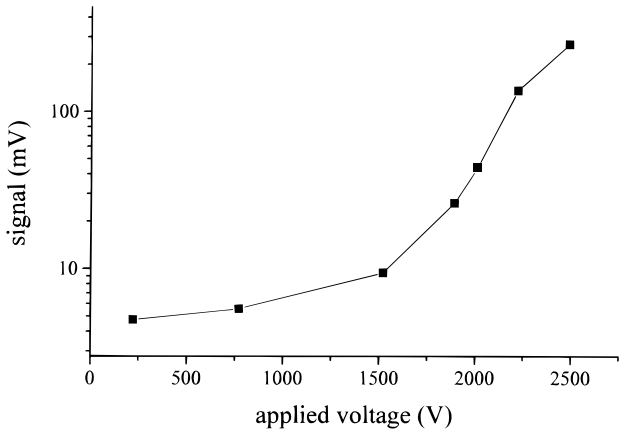

Figure 5. Behavior of the ionization signal vs applied high voltage showing the avalanche amplification effect. Ar was used as the inert carrier gas.

$n = 10$, a moderate increase in signal was achieved with increasing temperature, while a more significant dependence was seen for $n = 11$. On the contrary, for $n = 12$, the signal showed almost no dependence on temperature, and even a slight decrease at higher temperatures.

Although a quantitative explanation of the above results is not possible on the basis of the few data available, a qualitative interpretation can be attempted on the following grounds. First, it is reasonable to assume that, for $n = 10$ and at high laser energies, photoionization rather than collisional ionization is the dominating mechanism of the production of charges (see Figure 3). There is no doubt that collisions from the final excited level contribute to the signal but, at these temperatures and laser energies, this contribution is negligible compared to photoionization. Moreover, the data reported in Figure 3 allow one to speculate about the relative magnitudes of the photoionization and excitation cross sections for the 7s $^3S_1$ level reached with λ_{23}.

In our previous, time-resolved ionization study,[12] it was shown that direct photoionization from the 7s $^3S_1$ level occurred, as the ionization wave form observed without λ_{34} ($\lambda_{12} + \lambda_{23}$ only) resembled the exciting laser pulse shape. The behavior observed here as a result of increasing the laser energy of λ_{34} indicates that the excitation cross section for the 7s $^3S_1 \rightarrow n$p $^3P_0{}^2$ transitions ($n = 10$, 11, and 12) cannot differ from the photoionization cross section from the same 7s $^3S_1$ level in the absence of λ_{34} by more than ~1 order of magnitude. The high value of the photoionization cross section from the 7s $^3S_1$ level could be explained by the existence of autoionization states, i.e., discrete levels lying above the ionization continuum.

The different behavior of levels $n = 10$, 11, and 12 with temperature seen in Figure 4 can be attributed to a complex interplay between several parameters such as energy difference with the ionization continuum and nonionizing, quenching collisions, which have opposite effects on the magnitude of the signal. For $n = 10$, 11, and 12, it appears that quenching, collisional ionization, and photoionization are all contributing, but our present data do not allow us to extract each individual contribution to the overall signal. For the data presented in Figure 4, where a less focused laser was used, photoionization probably plays only a small role. The significant increase in ionization that is observed in going from $n = 10$ to $n = 12$ (at low temperatures) further supports this conclusion. To summarize these speculations, with lower laser irradiance, one can assume that collisional ionization is the dominant ionization process for $n = 10$ and 11 and the larger number of collisions at increasing temperatures results in an increasing signal, while for $n = 12$, quenching may dominate over the other processes at higher temperatures.

In view of the fact that, at low temperatures, the signal observed for $n = 12$ was the largest, and also because in this case λ_{34} (498.064 nm) lies at the peak of the gain curve of the dye, this Rydberg level was used in all subsequent experiments.

Avalanche Amplification. The experiments for optimizing the avalanche amplification of the signal employed the electrode configuration shown in Figure 2b because the configuration in Figure 2a resulted in noise and an electrical breakdown occurring between the two electrodes, which could result in destruction of the preamplifier. With the configuration in Figure 2b, voltages of up to 3 kV could be used without any onset of electrical breakdown occurring.

The avalanche amplification studies were carried out with an inert gas flow of <2 mL/min. In addition, an extra line of Ar gas was introduced to the cell to further dilute the number of Hg atoms and reduce space charge effects.

The first avalanche amplification studies involved the use of Ar as the inert gas. The results of this study are shown in Figure 5. This figure shows the classical behavior of an avalanche effect;[15,16] i.e., the signal remains relatively constant until it reaches a threshold level where an avalanche amplification, which is linearly related to the initial number of charges created, begins to appear. This behavior remains linear until it starts to be affected by the onset of some other behavior, such as space charge effects due to the presence of a large number of electrons between the electrodes or electrical breakdown. However, Ar resulted in an amplification factor of only 50 before electrical breakdown occurred. In order to increase this factor, as reported in a previous work,[11] Ar was replaced with P-10 gas.

The results of the study using P-10 gas are shown in Figure 6. In curve 1, the avalanche amplification obtained with three laser-connected steps is shown. Typical behavior was seen up to a high voltage of ~2000 V. At this point, space charge effects began to dominate and the proportionality with the initial number of charges was lost.[15,16] In order to avoid these effects, for applied high

(15) Blum, W.; Rolandi, L. *Particle Detection with Drift Chambers*; Springer-Verlag: New York, 1994.
(16) Rossi, B. B.; Staub, H. H. *Ionization Chambers and Counters*; McGraw Hill: New York, 1949.

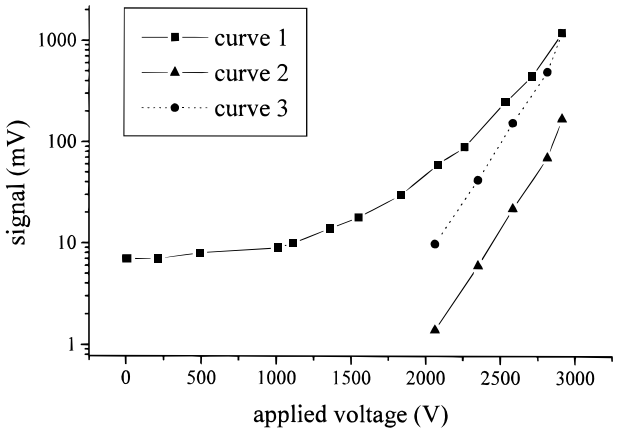

Figure 6. Same as Figure 5, but using P-10 as the inert carrier gas. Curve 1 shows the behavior for the three-step excitation, curve 2 shows the two-step excitation behavior, and curve 3 shows the normalization of curve 2 to the level of the three-step amplification.

voltages above 2000 V, the ionization signals generated using only the first two laser-connected steps were observed. The voltage dependence of this signal is shown in curve 2 and has been normalized to the three-step results in curve 3. In this way, the influence of space charge effects was avoided and the expected sharp rise in the signal with high voltage (HV), due to the avalanche effect, was restored. The amplification factor for the HV region where three steps could be utilized was 7.5, and the remainder of the amplification, achieved with just the two steps, was 121. This results in a total amplification factor of 7.5 × 121 or 908.

In order to ensure that the avalanche-amplified signal was related to the initial number of charges created as a result of the ionization of Hg atoms in the laser-irradiated volume, a spectral scan of the second laser step was performed at applied high voltages of 0.5 and 2.7 kV for the electrode configuration shown in Figure 2a, and of 3 kV for the configuration in Figure 2b. These results are shown in Figure 7. When panels b and c are compared, it is clear that the second electrode configuration (Figure 2b) not only prevented electrical breakdown from occurring but also resulted in a decrease of the random fluctuations of the signal observed at high voltages. The smoothed and normalized spectral profiles for λ_{23} are shown in Figure 8. The close resemblance between the spectral shapes of the avalanche-amplified signal and the signal observed at low voltages (where no avalanche amplification occurs) is a clear indication that the former signal carried the same direct proportionality with the initial number of charges (i.e., Hg atoms) created as did the latter.

Limit of Detection. The overall efficiency of ionization (collisional + photo) for the different excited Rydberg levels (n = 10, 11, and 12), η_{Ry}, can be estimated from the magnitude of the ionization signals obtained with and without λ_{34}, with the assumption that, when λ_{34} is absent, the signal is due only to photoionization.

The reported value of the cross section for photoionization (σ_{pi}) from the 7s $^3S_1$ level is 5.3 × 10^{-18} cm^2.[17] The wavelength for λ_{23} was 435.832 nm, which corresponds to 2.84 eV or 2.2 × 10^{18} photons J^{-1}. Because λ_{23} had an energy of 22 μJ and a beam diameter of 0.0312 cm^2, this corresponds to 4.84 × 10^{13} photons or 1.55 × 10^{15} photons cm^{-2}. For these measurements, the pulse energy of λ_{23} was reduced to 22 μJ in order that the enhancement factor due to the addition of λ_{34} could be measured without exceeding the linear range of the preamplifier. The efficiency of photoionization from the 7s $^3S_1$ level (two-step excitation) is defined here as the product of the laser photon fluence, E_{ph} (photons cm^{-2}), at λ_{23} and the photoionization cross section, i.e.

$$\eta\ (\text{2-step}) = E_{ph}\sigma_{pi} \qquad (1)$$

The use of the above values gives an efficiency of 0.0082 (0.82%).

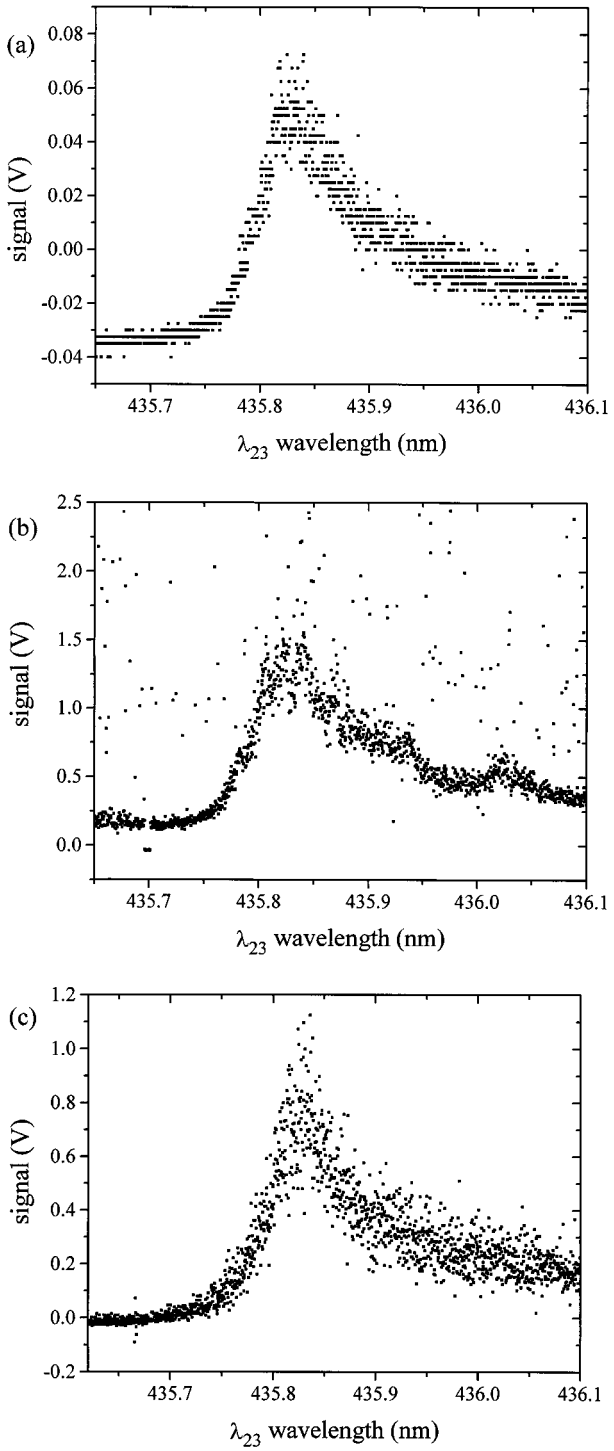

Figure 7. Spectral profiles for λ_{23} at applied high voltages of (a) 0.5, (b) 2.7 (avalanche amplification), and (c) 3 kV [avalanche amplification, alternate electrode configuration (Figure 2b)].

(17) Saloman, E. B. *Spectrochim. Acta Part B*, **1991**, *46*, 367−72.

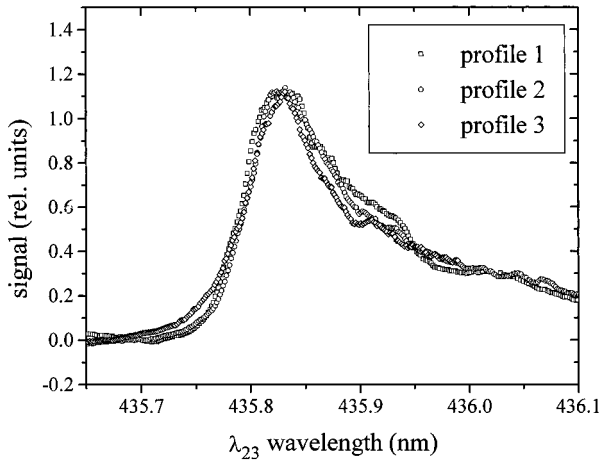

Figure 8. Smoothed and normalized spectral profiles for λ_{23}. Profile 1 is the smoothed profile shown in Figure 7b, profile 2 is the smoothed and normalized profile shown in Figure 7a, and profile 3 is the smoothed and normalized profile shown in Figure 7c.

The enhancement factor, EF, for the three-step excitation (n = 12) over the two-step excitation was calculated as

$$\mathrm{EF} = \mathrm{signal}(\lambda_1 + \lambda_2 + \lambda_3)/\mathrm{signal}(\lambda_2 + \lambda_1) \qquad (2)$$

From the experiment, a value of 32.3 was calculated for n = 12. Since the spectral irradiance of both λ_{12} and λ_{23} was more than sufficient to saturate the two Hg transitions, the overall ionization efficiency from 12p $^3P^0_2$ can be calculated as

$$\eta_{\mathrm{Ry}}(\text{3-step}) = \eta(\text{2-step})\mathrm{EF}\frac{g_3}{g_1 + g_2 + g_3} \qquad (3)$$

where g is the statistical weight of the first (g_1), second (g_2), and third (g_3) levels. In this way, η_{Ry} for n = 12 is calculated to be 0.11 (11%). It is important to point out that further increase in the laser energy density for λ_{34} led to the appearance of a background signal due to multiphoton ionization of the buffer gas; the calculated ionization efficiency of 0.11 corresponds to the best measurement with minimal background. The values calculated similarly for n = 10 and 11 are 0.051 and 0.055, respectively.

It is now possible to estimate a limit of detection (LOD) for n = 12 with avalanche amplification of the signal. The preamplifier used in this study was previously calibrated and produces 0.15 μV/electron.[18] The amplifier noise-limited LOD was determined to be 1500 electrons. With an avalanche amplification factor of 908, this corresponded to 1500 e^-/908 or 1.65 electrons/laser pulse. For n = 12, with an ionization efficiency of 0.11, this corresponded to (1.65 e^-/pulse)/(0.11 e^-/atom) or ~15 atoms/pulse in the laser-irradiated volume. It is important to emphasize that this was for a single pulse measurement. Typical signal-averaging procedures would have provided substantial S/N enhancement. While this calculation shows that our technique provides the most sensitive detection ever reported for mercury atoms in a cold environment, much work is needed to validate this result experimentally. Indeed, due to Hg contamination of the system, a background signal of approximately 10^3–10^4 Hg atoms in the interaction region was observed. This background could not be eliminated from our present setup.

CONCLUSIONS

It has been shown that a detection limit of several atoms in a single laser pulse can be attained for the LEI detection of Hg atoms in P-10 gas at ambient temperature. This is possible due to an avalanche effect which increases the signal by nearly 3 orders of magnitude. Direct proportionality with the initial concentration of atoms is maintained over a large dynamic range. This avalanche effect provides a detection capability of ~1.6 e^- during a single laser pulse.

Future work will take two directions. The first will include the optimization of the system to achieve single-atom detection. This will address improving the efficiency of ionization and increasing the amplification factor at atmospheric pressure. The second direction will be the validation of the technique from a practical analytical standpoint. In order to accomplish this, the Hg background needs to be greatly reduced and the linear dynamic range of the technique assessed. The method will then be applied to real samples of environmental interest, for example, to the direct determination of Hg in air and water.

ACKNOWLEDGMENT

The authors thank the U.S. Department of Energy which funded this research (DE-FG05-88-ER13881). W.C. thanks the U.S. Environmental Protection Agency for a research fellowship (U-914941-01-0). O.M. thanks the National Research Council for a Cooperation in Applied Science and Technology (CAST) grant.

Received for review February 24, 1997. Accepted April 15, 1997.[⊗]

AC9702148

(18) Riter, K. L.; Clevenger, W. L.; Mordoh, L. S.; Matveev, O. I.; Smith, B. W.; Winefordner, J. D. *J. Anal. At. Spectrom.* **1996**, *11*, 393–9.

[⊗] Abstract published in *Advance ACS Abstracts*, May 15, 1997.